Supporting Information

Transfer Printing Gold Nanoparticle Arrays by Tuning the Surface Hydrophilicity of Thermo-Responsive Poly N-isopropylacrylamide (pNIPAAm)

Sirous Khabbaz Abkenar, Ali Tufani, Gozde Ozaydin Ince, Hasan Kurt, Ayse Turak, and Cleva W. Ow-Yang*

1. Details of the materials synthesis procedures

Preparation of the gold nanoparticle arrays: The gold precursor, $HAuCl_4 \cdot xH_2O$ (Aldrich, 254169), was loaded into PS-b-P2VP diblock copolymer (Polymer Source, P10491-S2VP, M_w 183k-b-52k) reverse micelles dispersed in a toluene solvent. The loaded micelles were deposited onto silicon wafer substrates by spin coating (5500 rpm, 40 seconds). The polymeric matter was removed by oxygen plasma etching (O_2 at 30 sccm, 29.6 W RF power, 90 minutes; Harrick PDC-002, Ithaca, New York), and the gold precursor was reduced to elemental gold. In order to remove residual polymer on the sacrificial substrates, the post-etch substrates were subjected to further sonication processing in acetone, methanol and isopropyl alcohol (IPA) each for 10 minutes, respectively.

Deposition of the pNIPAAm films: PNIPAAm films were deposited by initiated chemical vapor deposition. The monomer N-Isopropylacrylamide (NIPAAm), the cross-linker ethylene glycol dimethacrylate (EGDMA) and the initiator tert butyl peroxide (TBPO) were used without further purification. The NIPAAm and the EGDMA were heated to 75 °C and 85 °C, respectively, to achieve sufficient vapor pressure, while the TBPO was kept at room temperature. The vapors were introduced into the evacuated deposition chamber at 1 mTorr. The optimized flow rates for pNIPAAM and EGDMA were 1 sccm and 0.075 sccm, respectively, while the flow rates of TBPO and N_2 were fixed at 1 sccm. The substrate and filament temperatures were set at 25 °C and 300 °C. Depositions were carried out under a

reactor pressure of 200 mTorr. The films thickness was monitored *in-situ* using a laser interferometry system to reach the target thickness of 100 nm.

PDMS stamp preparation: PDMS stamps (Sylgard 184, SIGMA-ALDRICH No. 761036) were prepared by mixing 8 g of base and 0.8 g of curing agent for 20 minutes. The solution was then degassed in an evacuated desiccator for 24 hours, cast into a glass petri dish, and then cured at 80 °C for 4 hours.

2. Spatial point pattern analysis for quantifying the array characteristics on the sacrificial substrate before transfer printing

The array of gold nanoparticles on a silicon substrate was imaged using secondary electrons in a field-emission scanning electron microscope (FE-SEM, LEO Supra VP-55). The images were processed (*i.e.* difference in image contrast amplified), in order to allow the use of the ImageJ software[1] to quantify the array characteristics—the average interparticle spacing and particle size distribution—by spatial point pattern analysis.[2]
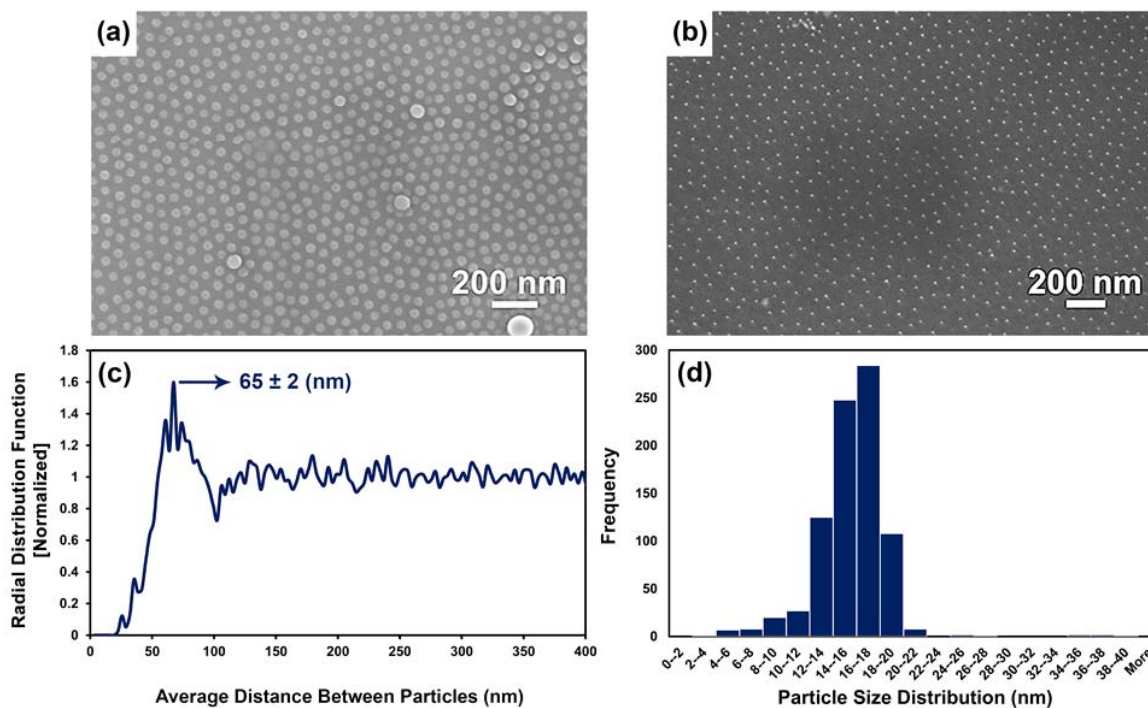
Figure S1. Original raw secondary electron images of a) gold precursor loaded diblock co-polymer micelles; b) the post plasma-etched GNP array on the sacrificial substrate; c) Radial distribution function and d) Particle size (diameter) distribution of GNPs on the sacrificial substrate.

3. Sacrificial substrate after pick-up at 5 °C
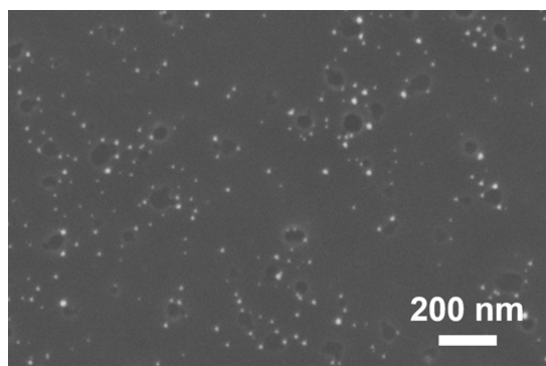

Figure S2. Original raw secondary electron image of the sacrificial substrate after pick up at 5 °C.

4. pNIPAAm surface and spatial point pattern analysis of the array transfer-printed onto the target substrate after transfer printing
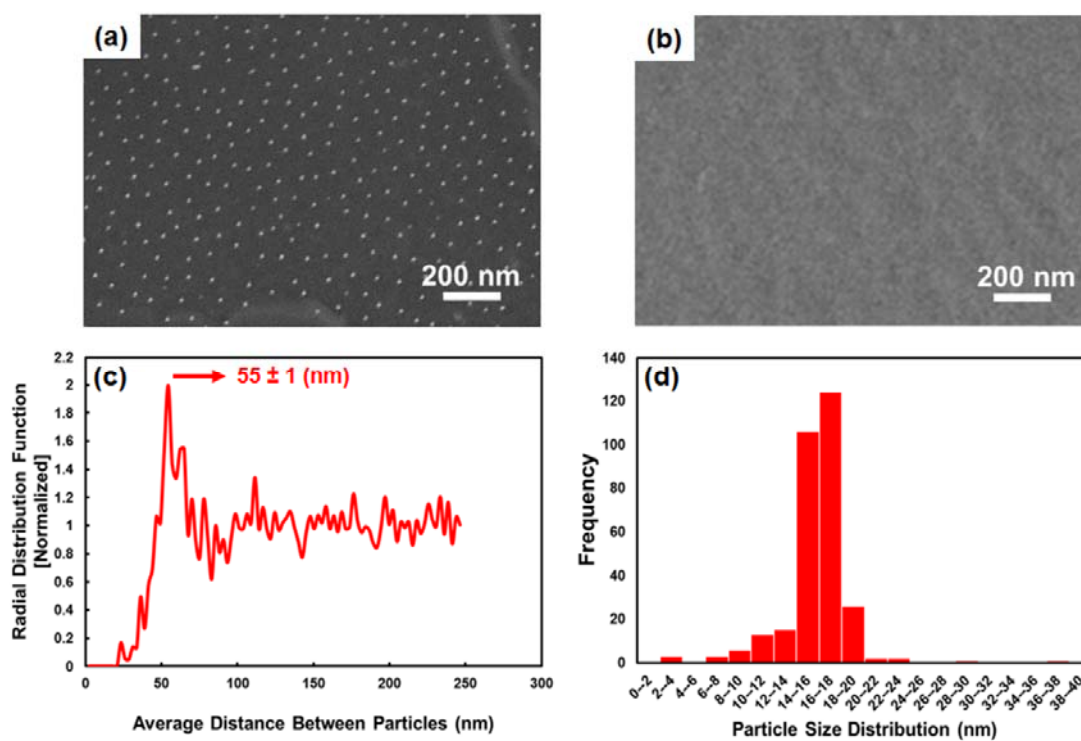

Figure S3. Original raw secondary electron images of a) the target transfer substrate; b) pNIPAAm surface after transfer to the target substrate at 50° C; c) the radial distribution function and c) the particle size (diameter) distribution of the transfer printed gold nanoparticle array.

5. Summary of array characteristics quantified by spatial point pattern analysis
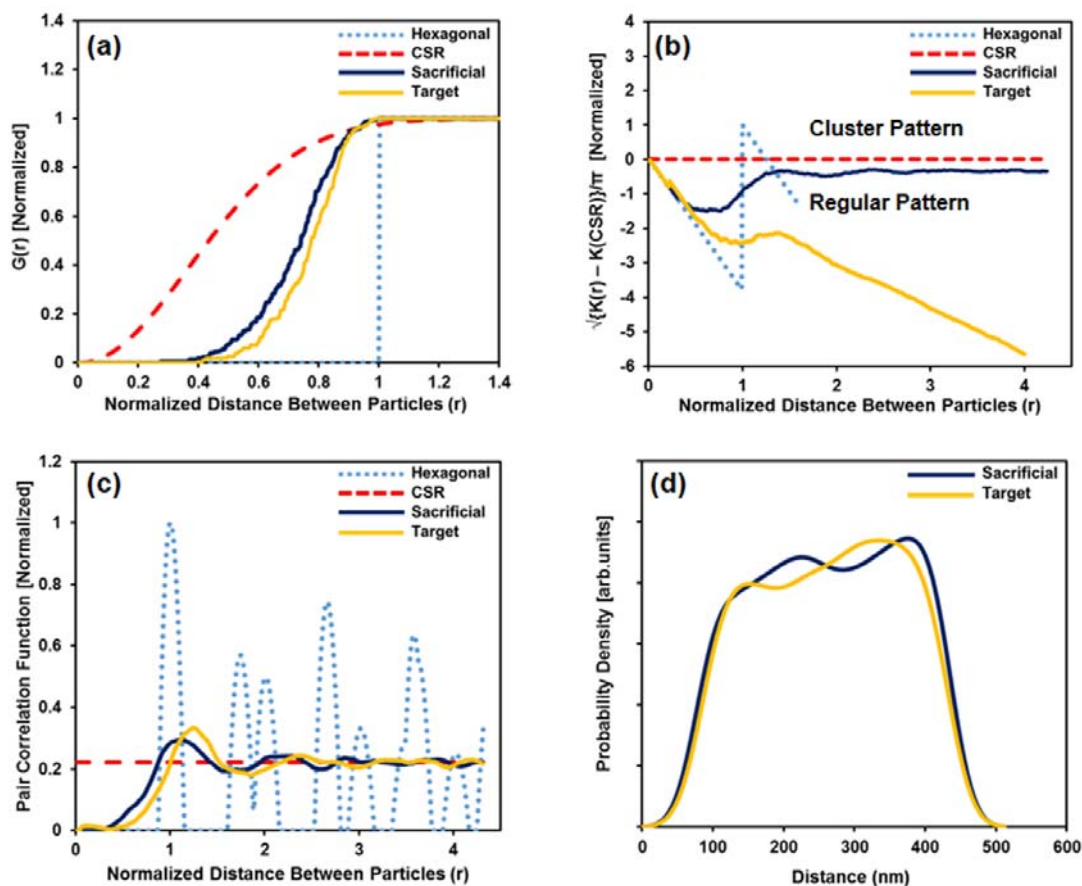

Figure. S4. Spatial point pattern functions for sacrificial and transfer substrate. All are normalized to a hexagonal lattice dispersion with similar interparticle distances and density of particles per unit area. Expected values for complete spatial randomness (CSR) and the 2D hexagonal close packed lattice are also given for comparison. a) Cumulative nearest neighbor distribution function ($G(r)$); b) Difference spectrum for the linearized Ripley's K function compared to CSR (dotted red line): clustered patterns lie above the CSR line, while ordered regular patterns fall below the line; c) pair correlation function; d) Distribution of nearest neighbors showing the three nearest neighbor peaks for the sacrificial and target substrates, which indicate the preservation of the same order after transfer printing.

6. Wetting contact angle measurements of pNIPAAm at 5 °C and 50 °C

We measured the wetting contact angle of sessile drops by using an optical tensiometer (Attension Theta Lite, Biolin Scientific AB, Stockholm, Sweden). Images were continuously recorded of the deionized water droplet from initial contact until it became stable, at a rate of 15 frames per second for 10 seconds, in the OneAttension version 2.3 software. To determine the contact angle, the captured images were automatically analyzed in the software by fitting the drop profile. The mean wetting contact angle was then calculated from the average contact angle extracted from all images captured during those ~10 seconds. The contact angle was measured on pNIPAAm at room temperature and at 50 °C. In order to perform the measurement of pNIPAAm at 50 °C, an electrically controlled heating plate (ThermoPlate, TOKAI HIT, Shizuoka-Ken, Japan) was mounted onto the sample stage, and the pNIPAAm-coated substrate was placed on top of the stage plate, once the plate had reached a stable 50 °C.

These images show that the degree of surface wetting on the pNIPAAm at room temperature is more hydrophilic (Figure S5a) than pNIPAAm at 50 °C (Figure S5b).
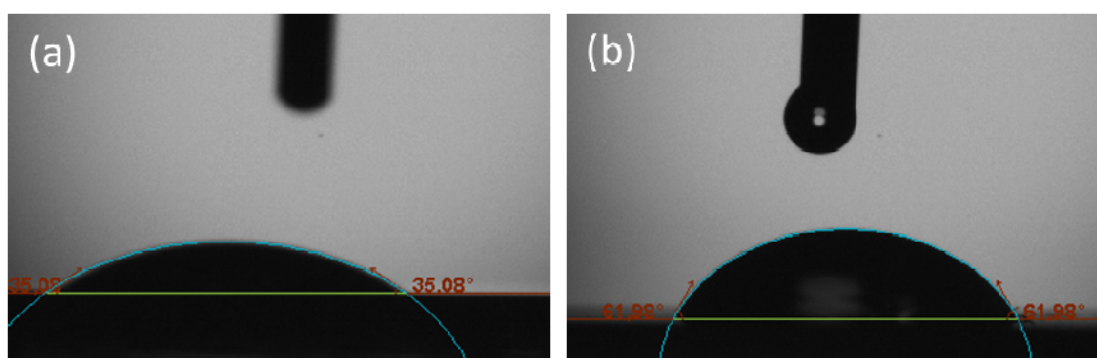

Figure. S5. Contact angle measurements on different regions of the pNIPAAm deposited on PDMS stamp. a) below the LCST at 25 °C and b) above the LCST at 50 °C.

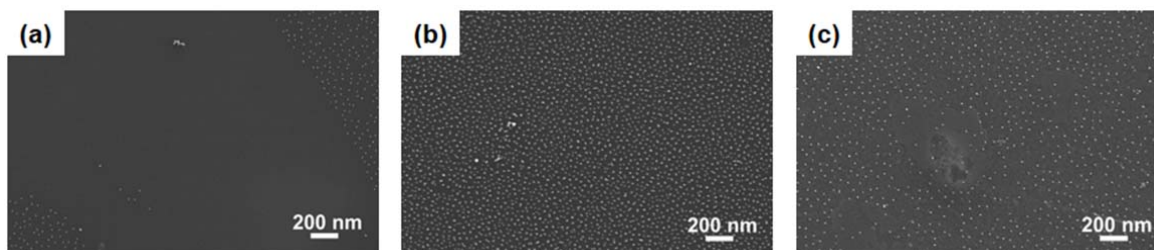## 7. Unprocessed) SEM images of the confirmation experiments

Figure S6. Original raw secondary electron images of a) sacrificial substrate after transfer printing at 5 °C; b) sacrificial substrate after transfer printing at 50 °C and c) target substrate after transfer printing at 50 °C, indicative of GNPs pick up only at 5 °C and GNPs release only at 50 °C.

8. Atomic force microscopy of the pNIPAAm film: lateral uniformity of surface morphology and elasticity

Samples of 10 mm x 10 mm size were mounted onto magnetic disks using double-sided adhesive tape. PeakForce QNM (Quantitative Nanomechanical Mapping) atomic force microscopy (AFM) mode and Bruker Multimode 8 was used to record surface topology, elastic modulus and adhesion maps. AFM measurements were performed using standard ScanAsyst-Air tips with resonant frequency of 70 kHz and spring constant of 0.4 N/m. Tip parameters were extracted from rough Ti reference substrate for tip shape and radius, sapphire reference substrate for cantilever deflection sensitivity using Nanoscope Analysis 1.40 software. The parameters further confirmed using low density polyethylene and polystyrene substrates. pNIPAAm surfaces were imaged using a scan size of 10 μm and a scan rate of 0.5 Hz. For validity of elastic modulus measurements, a minimum of 2 nm deformation is provided by adjusting peak force set point. All measurements were made under ambient conditions at room temperature and relative humidity of 50-60%. Gwyddion 2.44 and Nanoscope Analysis 1.40 software were used to process the obtained maps.
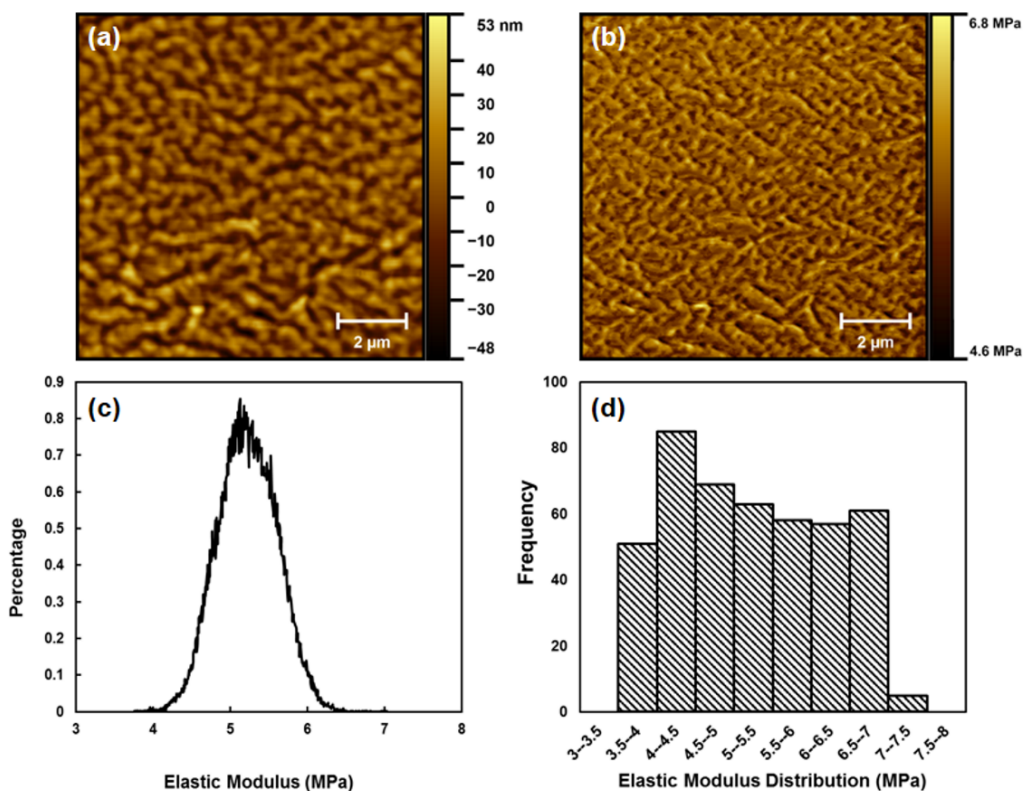
Figure. S7. Atomic force microscopy images of the pNIPAAm at room temperature: a) topography map and b-d) elastic modulus distribution.

FFT of the images allow semi-quantitative comparison of spatial frequencies present in the images. To correlate the wrinkles on the stamp with the regions of transferred GNP arrays, the spatial frequencies in the AFM height image of the stamp (Figure S8*a* and *b*) is compared with those in a processed version of the SEM image of the transfer-printed, target substrate (Figure S8*c* and *d*). Represented by the limits of frequency distribution in the 2-D FFT patterns, the spread in spatial frequencies in the area covered by the GNPs is consistent with the spread of the same in the wrinkles on the stamp surface.
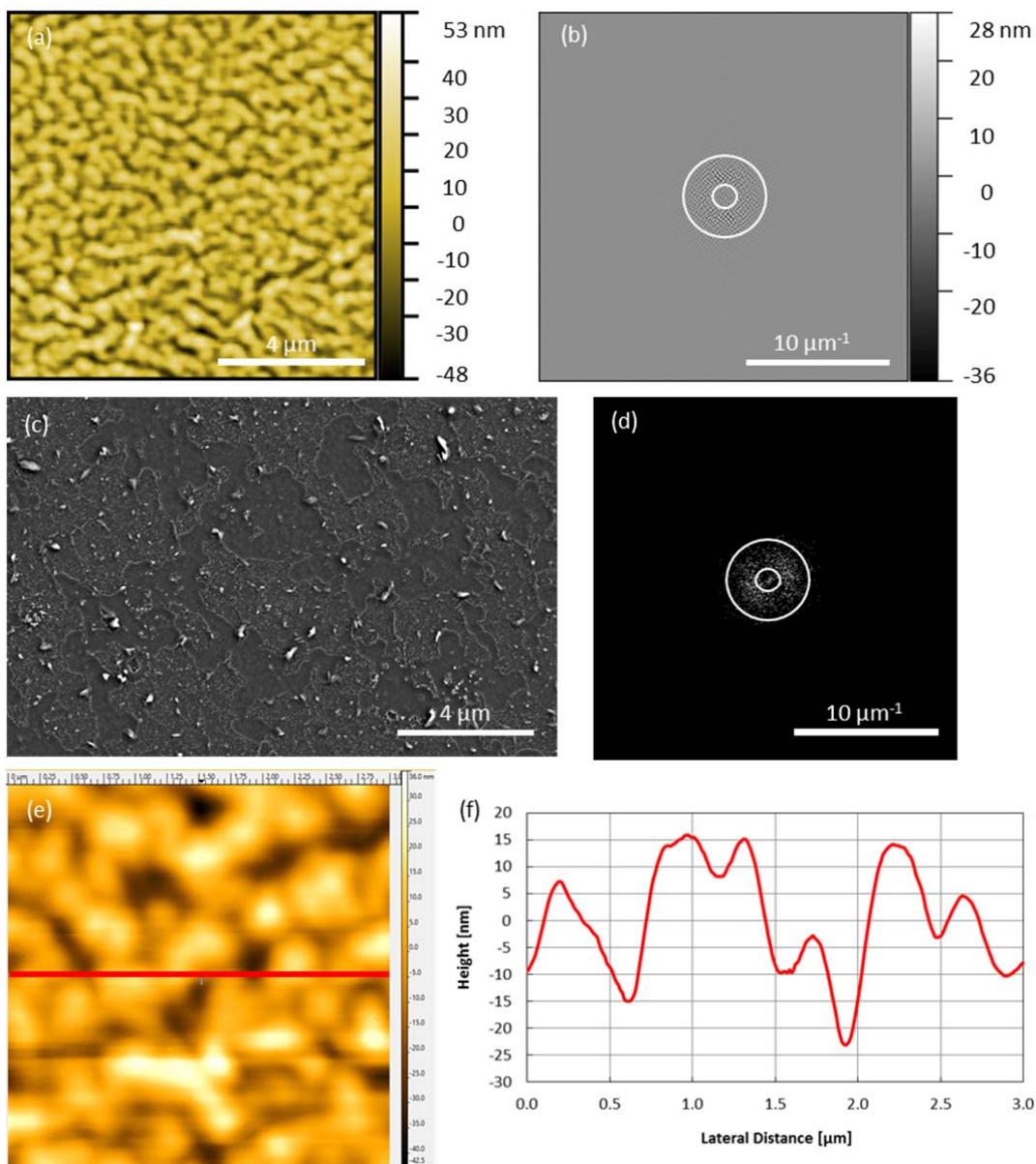
Figure S8. a) AFM height image of the pNIPAAm surface, b) FFT of AFM height image, c) SEM micrograph of a target substrate containing GNPs, d) FFT of the processed SEM image in part c; e) AFM height image of the pNIPAAm surface at higher magnification with f) line profile of height variation as indicated by the red line.

9. Ellipsometric thickness measurements of the pNIPAAm stamp upon heating up to 50 °C

Ellipsometry analysis (M2000 Spectroscopic Ellipsometer, J.A. Woollam Co., Inc.) was also carried out to confirm the volumetric transition of the pNIPAAm upon heating in the dry state in an ambient humidity of 70% RH.
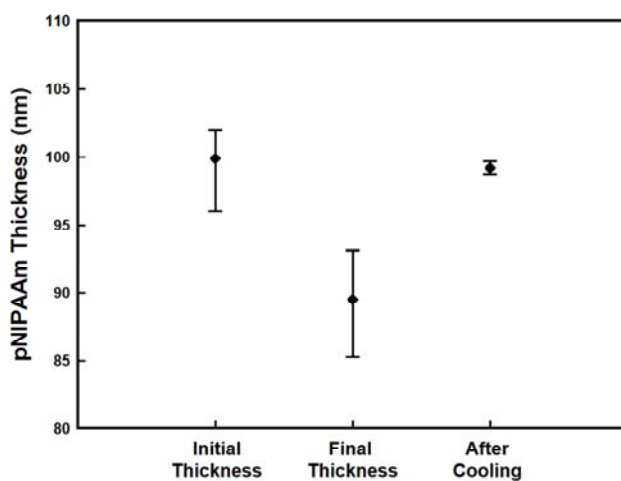

Figure S9. Variation in the thickness of pNIPAAm film upon heating from 25 °C up to 50 °C measured at three different locations on the same pNIPAAm film surface at ambient pressure.

10. Uniaxial loading of a bare PDMS stamp on sacrificial silicon wafer substrate

A dynamometer was placed beneath the upper plate of a custom-built uniaxial loading system and a PDMS film deposited onto a silicon wafer substrate. The dimensions of both PDMS and silicon wafer were 2 cm x 1 cm. Pressure was applied constantly up to the fracture point of silicon wafer substrate and the normal force versus time was monitored on the screen. At the fracture point, a force of 180 N was recorded by the dynamometer.
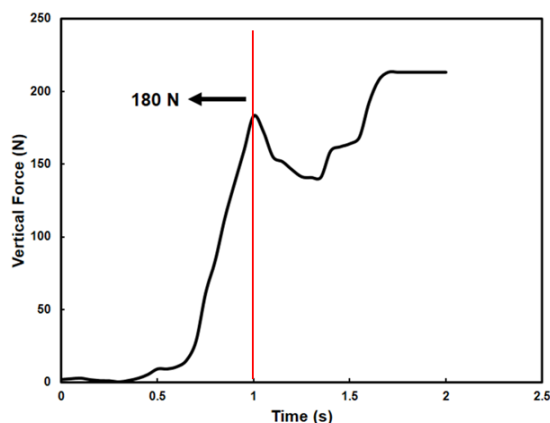
Figure S10. Vertical force of a home-made pressure device versus time for a PDMS stamp (1×2 cm) on a sacrificial silicon wafer substrate (1×2 cm). Sudden decrease in force indicates the fracture of silicon wafer substrate at a pressure of 900 kPa.

11. The incorporation of transfer printed of gold plasmonic particles into PCDTBT:PC70BM bulk heterojunction (BHJ) polymer solar cells

We integrated the transfer-printed GNP array interlayers into poly[N-9'-heptadecanyl-2,7-carbazole-alt-5,5-(4',7'-di-2-thienyl-2',1',3'-benzothiadiazole)]:[6,6]-Phenyl-C71-butyric acid methyl ester (PCDTBT:PC$_{70}$BM) bulk heterojunction (BHJ) devices. Pre-patterned indium tin oxide anode substrates (ITO, Ossila S101, Sheffield, UK) with and without GNP arrays were sonicated in acetone, methanol and isopropanol baths for 10 min each, prior to 30 min. UV-ozone treatment. A thin layer of diluted poly(3,4-ethylenedioxythiophene):polystyrene sulfonate (PEDOT:PSS, Heraeus Clevios^{TM} PVP AI 4083, filtered at 0.45 μm) was deposited by spin-coating (6000 rpm, ~30 nm thickness) and annealed at 150 °C for 15 min under ambient conditions. PCDTBT (Ossila M137, Sheffield, UK; M$_w$ 42200) and PC$_{70}$BM (Ossila M113, Sheffield, UK; 95%) were mixed in a 1:4 weight ratio in chlorobenzene. PCDTBT:PC$_{70}$BM (20 mg/mL) solution was deposited by spin-coating at 3000 rpm for 60 s, resulting in a ~70 nm thick layer. Layer thicknesses were measured using a surface profiler (KLA-Tencor P6, Milpitas, CA, USA). The samples were fabricated in ambient clean room

11

conditions and immediately transferred to a thermal evaporator chamber and placed under high vacuum ($< 2x10^{-6}$ mbar). To make the back-side electrical contact, we performed thermal evaporation of a 1.3 nm-thick LiF layer, followed by a 100 nm-thick Al cathode layer on the organic active layers. The samples were then annealed at 80 $^{\circ}$C for 15 min. after cathode evaporation under vacuum. The devices were subsequently encapsulated using UV-curable epoxy (Ossila E131, Sheffield, UK) and cured under 365 nm UV illumination.

GNPs show plasmonic behavior, which lead to field amplification, light scattering and light absorption—i.e., enhancing the interaction between incident sunlight and the active layers in photovoltaics. When nanostructures are significantly smaller than the wavelength of the incoming light, collective oscillations of electrons formed over the surfaces of nanostructures become localized, rather than propagating. Thus, the localized surface plasmon resonance (LSPR) behavior in GNP arrays can be exploited in light-trapping and field transmission-amplification strategies in photovoltaics in order to improve device performance.[3,4]

We evaluated the performance of bulk heterojunction polymer solar cells containing the transfer-printed GNP array at the ITO anode. **Figure S11** shows the J-V characteristics of PCDTBT:$PC_{70}BM$ solar cells under 1 sun illumination with and without transfer printed GNPs incorporated on the ITO anode. The transfer-printed GNPs improved the power conversion efficiency (PCE) of PCDTBT:$PC_{70}BM$ solar cells by 32.2%. The open circuit voltage (V_{oc}) was improved by 50 mV, and the photogenerated short circuit current (J_{sc}) was increased by 27.6%. Both parameters combined contributed to a slight reduction in fill factor (FF) from 48% to 47% (**Table S1**).

As a proof-of-concept, we have demonstrated the transfer printing of a plasmonic particle array onto the ITO anode of a PCDTBT:$PC_{70}BM$ BHJ OPV, during the device fabrication. The device performance was compared to one with an ITO anode, on which the plasmonic particle array was deposited directly in micelles and plasma-etched. Figure S10, summarizing the device characteristics, shows that the performance was not adversely impacted by the

transfer printing process. In the device containing a transfer-printed GNP array, the plasmonic enhancement led to a 32.2% improvement in PCE.
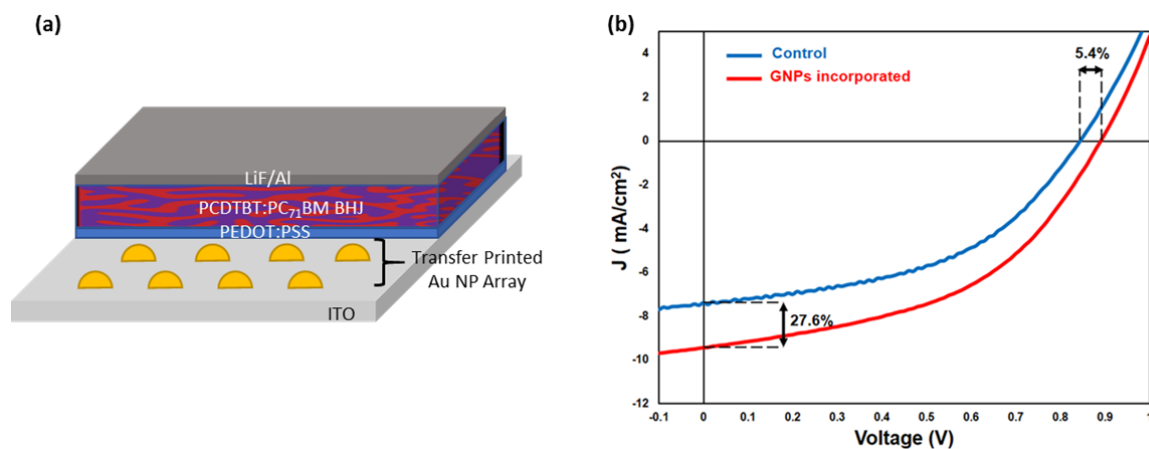

Figure S11. (a) Cross-sectional schematic of the plasmonic enhanced PCDTBT:PC$_{70}$BM solar cells, with a cut-away showing the location of the GNP layer; and (b) their *J-V* characteristics under 1 sun illumination, in comparison with devices without transfer printed GNPs, incorporated on ITO anode.

Table S1. Characteristics of the PCDTBT:PC$_{70}$BM solar cells with and without transfer printed GNPs on the organic active layer.

OPV	V_{oc} [V]	J_{sc} [mA cm^{-2}]	FF	PCE [%]
Control	0.844	-7.39	0.48	2.98
GNPs incorporated	0.890	-9.43	0.47	3.94

REFERENCES

1. C. A. Schneider, W. S. Rasband and K. W. Eliceiri, *Nat. Methods*, 2012, **9**, 671-675.

2. C. W. Ow-Yang, J. Jia, T. Aytun, M. Zamboni, A. Turak, K. Saritas and Y. Shigesato, *Thin Solid Films*, 2014, **559**, 58-63.

3. H. A. Atwater and A. Polman, *Nat. Mater.*, 2010, **9**, 205-213.

4.   H. Kurt and C. W. Ow-Yang, *Phys. Status Solidi A*, 2016, DOI: 10.1002/pssa.201600314.